

# Pedestrian Behavior Prediction for Automated Driving: Requirements, Metrics, and Relevant Features

Michael Herman, Jörg Wagner, Vishnu Prabhakaran, Nicolas Möser,  
Hanna Ziesche, Waleed Ahmed, Lutz Bürkle, Ernst Kloppenburg, and Claudius Gläser

**Abstract**—Automated vehicles require a comprehensive understanding of traffic situations to ensure safe and comfortable driving. In this context, the prediction of pedestrians is particularly challenging as pedestrian behavior can be influenced by multiple factors. In this paper, we thoroughly analyze the requirements on pedestrian behavior prediction for automated driving via a system-level approach: to this end we investigate real-world pedestrian-vehicle interactions with human drivers. Based on human driving behavior we then derive appropriate reaction patterns of an automated vehicle. Finally, requirements for the prediction of pedestrians are determined. This also includes a novel metric tailored to measure prediction performance from a system-level perspective. Furthermore, we present a pedestrian prediction model based on a Conditional Variational Auto-Encoder (CVAE) which incorporates multiple contextual cues to achieve accurate long-term prediction. The CVAE shows superior performance over a baseline prediction model, where prediction performance was evaluated on a large-scale data set comprising thousands of real-world pedestrian-vehicle-interactions. Finally, we investigate the impact of different contextual cues on prediction performance via an ablation study whose results can guide future research on the perception of relevant pedestrian attributes.

**Index Terms**—Autonomous vehicles, Automated driving, Prediction methods, Machine learning.

## I. INTRODUCTION

**R**OAD safety is a key driver for the development of driver assistance and automated driving systems. According to a report of the World Health Organization [1] traffic accidents cause more than 1.3 million fatalities annually, almost half of them being vulnerable road users (VRUs). Therefore, the protection of VRUs, in particular pedestrians, constitutes a major goal of intelligent vehicles. The Automatic Emergency Braking system for Pedestrians (AEB-P) is a good example on how driver assistance systems already protect pedestrians today. AEB-P detects pedestrians in the predicted vehicle's path and, if a collision cannot be avoided by the driver, automatically initiates emergency braking. By either avoiding the collision or, if avoidance is not possible, reducing the velocity of an impact, pedestrian AEB systems mitigate pedestrian fatality and injury [2]. The detection of pedestrians and the

M. Herman, J. Wagner, V. Prabhakaran, H. Ziesche, and E. Kloppenburg are with the Bosch Center for Artificial Intelligence, Germany.

N. Möser, L. Bürkle, and C. Gläser are with the Robert Bosch GmbH, Corporate Research, Germany.

W. Ahmed is with the Robert Bosch GmbH, Chassis Systems Control - Automated Driving, Germany.

e-mail: Michael.Herman@de.bosch.com



Fig. 1. Exemplary scenario in which the behavior of a pedestrian depends on multiple contextual cues, e.g. the present road infrastructure or interactions with other traffic participants.

prediction of their behavior are essential components of an AEB-P system. Prediction of an AEB-P is generally restricted to short prediction horizons in the order of 1 to 2s and is typically based on kinematic models.

On the other hand, automated driving not only addresses near-collision situations, but broadens the scope to everyday driving scenarios. Thus, besides collision mitigation, comfortable driving that imitates human driving behavior shifts into focus. This requires an extended pedestrian behavior prediction to correctly reason about a situation and react appropriately at an early stage. Long-term pedestrian prediction, however, constitutes a big challenge, since the behavior of pedestrians is influenced by many aspects. The exemplary scenario of a girl running along a sidewalk depicted in Fig. 1 illustrates this issue. The future behavior of the running girl is likely to depend on a variety of factors, e.g. the course of the sidewalk, the people on the sidewalk blocking her path, the trajectory of an approaching vehicle, and the presence of a zebra crossing. We thus argue that the behavior of pedestrians cannot be investigated independently, but rather has to be considered within the context of the overall traffic scene. This includes the static driving infrastructure (e.g. the road layout), interactions of the pedestrian with other traffic participants (e.g. an approaching vehicle), and appearance or communication cues (e.g. gestures).

In this paper, we derive requirements on pedestrian behavior prediction in the context of automated driving. In addition, we propose a prediction model that specifically addresses long-term prediction by taking into account contextual cues of the traffic scene. In detail, the contributions of the paper are:

- An appropriate system reaction pattern for interactions of

an automated vehicle with pedestrians is derived from an analysis of human driving behavior,

- Requirements for pedestrian behavior prediction in automated driving and a corresponding metric to assess prediction performance are specified,
- A pedestrian prediction model based on a Conditional Variational Auto-Encoder (CVAE) which incorporates various contextual cues is presented. The CVAE shows superior performance over a baseline prediction model, where prediction performance is evaluated on a large-scale dataset comprising thousands of real-world pedestrian-vehicle-interactions,
- Relevance of different contextual cues is assessed based on an ablation study.

The remainder of this paper is organized as follows: We first give an overview on related work in Sec. II. We then introduce our large-scale dataset of vehicle-pedestrian interactions in Sec. III. In Sec. IV we analyze pedestrian-vehicle interactions to determine human driving behavior and to derive requirements on pedestrian prediction for automated driving. Our prediction model is introduced in Sec. V and thoroughly evaluated in Sec. VI. Finally, we conclude the paper with a discussion of our results in Sec. VII.

## II. RELATED WORK

In this section, we give an overview of state of the art approaches as well as typical input features applied to pedestrian prediction. Furthermore, evaluation metrics and public datasets are briefly summarized. For a more comprehensive overview, we refer the reader to [3].

### A. Existing Models

Predicting future motion of traffic participants is an extensively studied field. Many traditional approaches depend on a set of explicitly defined dynamics equations that are generally derived from physics-based motion models [3]. Often, these approaches use Probabilistic Graphical Models to define these relations [4], [5], [6].

Recently, pattern-based methods that learn behavioral patterns from data have outperformed traditional approaches. Especially, deep learning based solutions became state of the art for most of the problems related to public datasets. Often, Recurrent Neural Networks (RNN) are used for encoding trajectories of interacting agents and decoding future behavior [7], [8], [9]. One of the major problems associated with these approaches is to accurately capture the probabilistic, multi-modal distribution over trajectories. In order to address this issue recent deep learning based methods predict parametric distributions [7], learn mixtures of Gaussian trajectory distributions [10], use adversarial training approaches [11], or introduce discrete [12] or continuous [13], [14], [15] latent variables. The models presented in this paper build on Conditional Variational Autoencoders (CVAE) [16], which use continuous latent variables to capture complex, multi-modal probability distributions.

### B. Used Features

Human behavior is influenced by contextual cues of internal and external stimuli. The survey [3] groups them into three categories: cues of the target agent, the dynamic environment, and the static environment. Potential target agent cues are the motion state (e.g. position, velocities) [6], [7], [9], appearance based cues (e.g. head or body pose) [17], or semantic attributes (e.g. age or gender) [18]. While traditional models often do not take into account influences of the dynamic environment [19], [20], [21], other approaches exist that model interactions with other agents [22], [23], [7] or even social groups [24]. Regarding cues of the static environment, there are several approaches that neglect this influence [25], [26], some others only model influence of individual static objects [27], while still others model more complex influences from environment geometry and topology [28], [29].

### C. Evaluation Metrics

Performance evaluation is an integral part of the process of creating a prediction model. The survey [3] extensively discusses different metrics for models that predict trajectories. These metrics fall into two classes, geometric and probabilistic. A widely used geometric metric is the average displacement error (ADE), which applies to models providing point predictions. ADE measures the euclidean distance of a predicted trajectory from ground truth positions at a specific prediction time interval, averaged over the trajectory, or over multiple trajectories. A common misuse of ADE is applying it to probabilistic predictions, averaging over the predictive distribution as well.

Probabilistic metrics are used for models that provide predictions in the form of probability densities. This kind of metrics measures how well the predictions capture the uncertainties inherent to the prediction process as well as the true process. A typical metric here is average (negative) log likelihood of the ground truth positions. Another example would be Kullback-Leibler divergence. Unfortunately, these kind of metrics tends to lack intuitive interpretability. One subtlety with the different probabilistic metrics is whether they encourage multimodal predictive distributions or not.

This leads to the question whether the metrics discussed so far measure properties relevant for possible applications of the model under consideration. [30] discuss the problem of evaluating generative (probabilistic) models and come to the conclusion that application specific metrics are generally required. This is done by [31] for a pedestrian prediction application. The authors pose their prediction task as an intent classification problem, and use a classification performance metric. A standard graphical classification performance metric for classifiers with binary predictions are ROC curves [32], with the related numerical metric AUC which measures the area under the curve. Classifiers that predict class probabilities allow for continuous numerical metrics like log loss [33], also known as cross entropy, which is widely used in machine learning.

D. Datasets

In contrast to the large number of datasets devoted to pedestrian detection there is only a limited number of datasets that address pedestrian prediction in automated driving context. Most notably the latter include the Joint Attention in Autonomous Driving (JAAD) dataset [34], the Pedestrian Intention Estimation (PIE) dataset [35], and the Daimler Pedestrian Path Prediction Benchmark dataset [36]. Each of them only covers video recordings, which renders them suitable to benchmark computer vision algorithms. However, they are limited in use for investigating trajectory prediction which is usually carried out in birds-eye view. Other datasets comprise such top-view trajectories (e.g. ETHZ dataset [37], Stanford Drone Dataset (SDD) [24]), but were recorded in non-automotive scenes. Recently, various large scale automotive datasets were published (e.g. [38], [39], [40], [41]), many of them comprising tracking or motion forecasting challenges, too. However, they mainly focus on the task of predicting other vehicles and thus lack a significant number of scenes that cover pedestrian-vehicle interactions. To overcome this shortage, we created a large-scale dataset that specifically addresses pedestrian prediction in automated driving context. We will introduce the dataset in the following section.

III. DATASET

A. Data Collection

The dataset we refer to in this paper comprises vehicle-pedestrian interactions from inner-city traffic in southern Germany. The data was recorded on four different round-courses with lengths between 2 and 4 km. The routes were chosen to maximize variability of traffic scenarios including both downtown and suburban areas, different road sizes, traffic densities, and number of pedestrians. Furthermore, the routes contain various traffic control elements which are relevant for vehicle-pedestrian interactions, most notably zebra crossings, pedestrian refuge islands, or a combination of both.

To further increase scenario coverage a number of actors were positioned at different locations along the courses. The instruction of actors followed a semi-scripted approach where actors were told not to perform specific interactions with the recording vehicle but rather to arbitrarily vary their walking routes, interactions and behavior in a realistic manner. Since actors had to adapt their behavior to the respective traffic situation, including the recording vehicle and other traffic

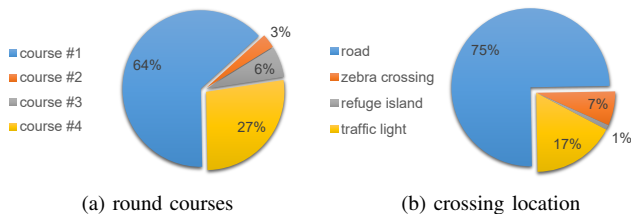


Fig. 2. Dataset statistics: (a) depicts the distribution of pedestrian tracks with respect to the four courses; (b) illustrates the locations at which pedestrians crossed the street.

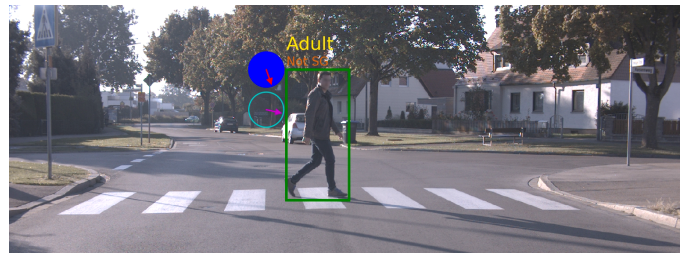


Fig. 3. Example of labeled pedestrian attributes: The compass plots depict head and body orientation, where the filled upper compass indicates that the pedestrian is looking at the ego-vehicle.

participants, the setup proved to result in a great variety of realistic vehicle-pedestrian interactions.

The recordings were carried out during three weeks in fall of 2018. Overall, we recorded 80 hours of data using different drivers to reduce driving style biases. Data acquisition was performed using a Bosch test vehicle equipped with various surround sensors. The recorded data comprises 3D point clouds of a 360 degree LiDAR sensor and images of two front-facing cameras with horizontal opening angles of 45 and 90 degrees, respectively. Furthermore, an IMU with differential GPS provides precise information on the ego-vehicle’s position and motion.

B. Data Labeling

Data post processing included an automatic extraction of pedestrian trajectories. As a first step, we applied pedestrian detectors on the recorded point cloud and image data, respectively. The detections from the different sensors were subsequently matched and finally tracked in 3D using Kalman filtering with constant velocity models. Overall, we could extract 99,011 pedestrian tracks from our recordings, out of which 7 % are crossing the road. Fig. 2 illustrates the distribution of tracks with respect to the different round courses and crossing locations. We finally excluded pedestrian tracks at traffic lights because behavior there is mostly deterministic given the traffic light states.

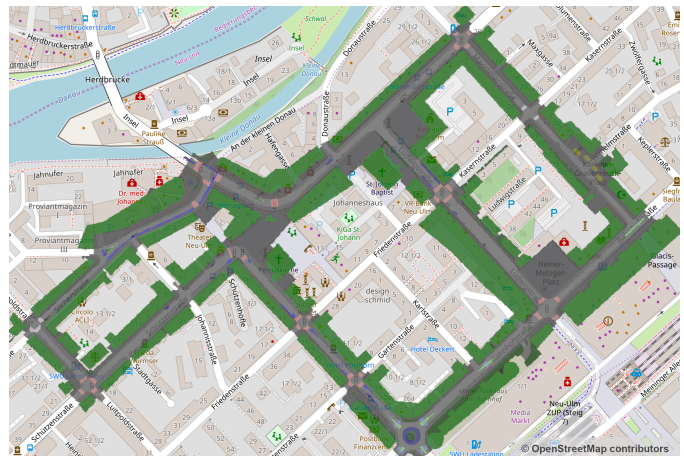
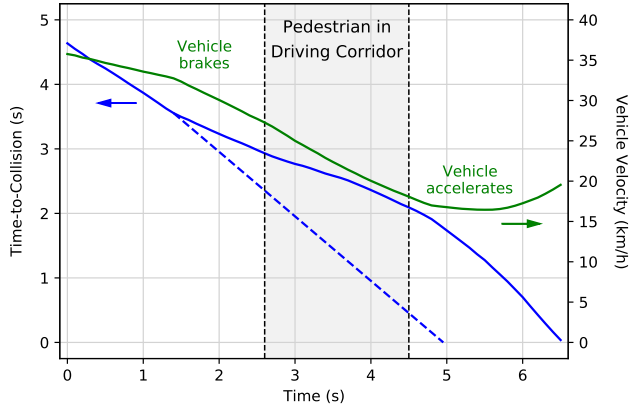
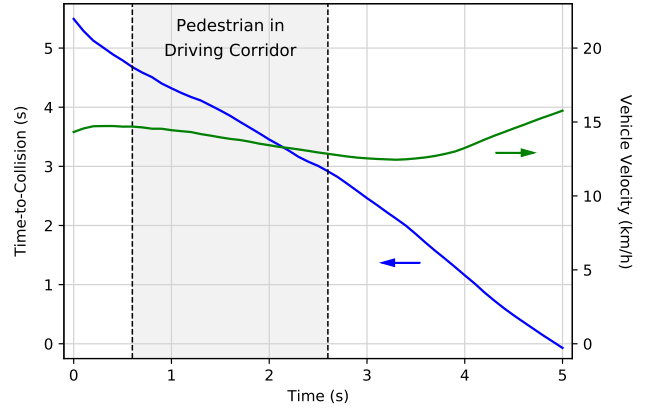


Fig. 4. Semantic map of one round course overlaid to a road map. Different colors denote different semantic classes.





(a)



(b)

Fig. 5. Two traffic scenarios of a vehicle approaching a pedestrian crossing the roadway. In scenario (a) the driver brakes in order to maintain a time-to-collision above approximately 2 s while the pedestrian is traversing the driving corridor of the vehicle. In scenario (b) the driver maintains a sufficiently large time gap between his vehicle and the pedestrian without having to brake.

To enable an investigation of potentially behavior-relevant features, we further performed hand-labeling of a subset of 10,159 pedestrians. For the labeling, the tracks were randomly selected while ensuring that tracks are balanced between crossing and non-crossing pedestrians as well as location (i.e. presence of different traffic control elements). As depicted in Fig. 3, the frame-wise labels include body and head orientation (in degrees).

Finally, we created semantic maps of the round courses via hand-labeling of decimeter-level accurate aerial orthoimages (see Fig. 4). These maps comprise the locations of roads, sidewalks, cycle tracks, bus lanes, barred areas, zebra crossings, refuge islands, traffic lights, lawn, and buildings. The trajectories of the ego-vehicle as well as those of the detected pedestrians hence can be projected onto the map, given the precise global position recordings of the ego-vehicle.

#### IV. REQUIREMENTS ON PEDESTRIAN BEHAVIOR PREDICTION

##### A. Analysis of Human Driving Behavior

In order to define a suitable system behavior of an automated vehicle, we investigated different scenarios where a human driver interacts with pedestrians crossing the roadway in front of the vehicle. These scenarios were taken from the dataset described in Section III. Two typical examples are depicted in Fig. 5.

A common measure for the criticality of a driving situation is the time-to-collision  $TTC = d/v$ . It is calculated from the

distance to an obstacle  $d$ , in our case a pedestrian, in relation to the driving velocity  $v$  and thus indicates the time required for a vehicle to hit the obstacle assuming constant velocity.

The graph in Fig. 5a shows the velocity (green) and the TTC (blue) of a vehicle approaching a pedestrian who crosses the road from left to right. The two vertical dashed lines at  $t_1 = 2.6$  s and  $t_2 = 4.5$  s mark the points in time at which the pedestrian enters and leaves the driving corridor of the vehicle, respectively. For the analysis in this paper we assume a driving corridor width of 3 m. Overall it takes the pedestrian 1.9 s to traverse the danger zone of the driving corridor. At time  $t_1$ , when they enter the corridor, the TTC of the approaching vehicle is 2.9 s and at time  $t_2$ , when the pedestrian leaves the corridor again, TTC is 2.1 s.

As soon as the driver recognizes that the pedestrian intends to cross the roadway, they slightly start to brake their vehicle at  $t = 1.5$  s. This can be clearly seen by the decrease in slope of the vehicle velocity and by the increase in slope of the TTC curves, respectively. By slightly braking, the driver maintains a TTC above approximately 2 s while the pedestrian is traversing the driving corridor. As soon as the pedestrian has left the corridor and is thus out of the danger zone, the driver releases the brake at  $t = 4.8$  s and shortly afterwards accelerates the vehicle.

In contrast, the dashed blue line in the graph indicates how the TTC would evolve over time if the driver did not brake and maintained a constant velocity. In this case, the vehicle would approach the pedestrian faster leading to smaller TTC



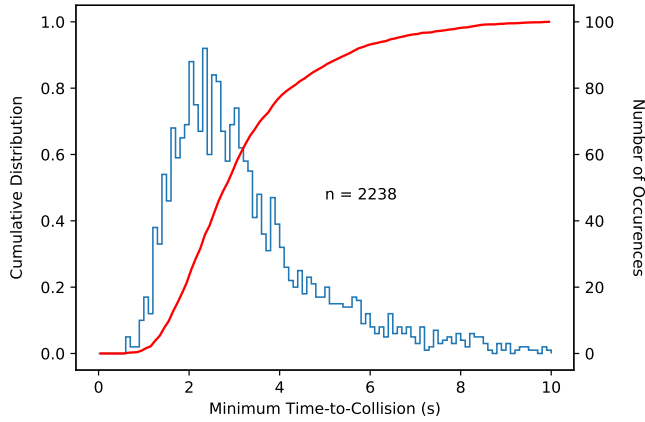


Fig. 6. Cumulative distribution function (red) and number of occurrences (blue) of the minimum time gap while pedestrians traverse the driving corridor of an approaching vehicle. The median of the distribution is at a minimum time gap of 2.84 s.

values while the pedestrian is traversing the driving corridor. Here, the TTC would drop to a value of 0.5 s at  $t_2$  when the pedestrian leaves the driving corridor.

Fig. 5b depicts another traffic scenario with a vehicle approaching a pedestrian crossing the roadway from right to left. Again, the dashed vertical lines indicate when the pedestrian enters and leaves the driving corridor, respectively. In contrast to the previous case, the driver neither brakes nor accelerates while their vehicle is approaching the pedestrian. This is due to the fact that the time gap already is at a safe level  $> 2.9$  s while the pedestrian is traversing the driving corridor and, therefore, the driver does not have to take any action but rather maintains a constant velocity of approximately 14 km/h.

These two examples suggest that human drivers try to establish a time gap between the pedestrian and their vehicle that does not fall below a certain threshold value for the time span while a pedestrian traverses the driving corridor. This hypothesis is also confirmed by a statistical analysis of the minimum time gaps which occur in crossing scenarios. To this end, 2,238 scenarios of pedestrians crossing the roadway from right to left and vice versa in front of an approaching vehicle were identified in the data set. For these scenarios, the minimum time gaps occurring while the pedestrians were traversing the vehicle corridor were determined.

Fig. 6 shows the cumulative distribution function (red) and the number of occurrences (blue) of these scenarios as a function of the minimum time gap. The onset of individual scenarios occurs at a minimum time gap of 0.6 s and the distribution reaches the maximum number of occurrences in the right-open interval between 2.3 s and 2.4 s. The median of the distribution is at a minimum time gap of 2.84 s, the first and third quartiles are at 2.09 s and 3.92 s, respectively.

The distribution function of minimum time gaps thus shows that drivers try not to fall below a certain threshold value for the time gap between their vehicle and the pedestrian crossing, which is perceived as safe and comfortable by both parties. If the initial situation of a crossing scenario leads to a time gap lower than the threshold value, the driver reacts by adjusting

the speed of their vehicle accordingly, e.g. by applying the brakes. Furthermore, the results show that a minimum time gap of at least 2.8 s (i.e. the median of the distribution) is perceived as safe and comfortable by the majority of traffic participants.

### B. Derived AD System Reaction Pattern

Based on our analysis of human driving behavior we next derive system reactions of an automated vehicle that should mimic those of human drivers. For the sake of simplicity we focus on longitudinal vehicle control, i.e. the adaption of the vehicle's velocity along a predefined or planned path. As shown in the previous section, the observed minimum time gap between a vehicle and a pedestrian traversing the driving corridor is of particular importance in this respect. Our analysis suggests, that there is a threshold value below which a situation is perceived uncomfortable or even critical. The acceptance of time gaps is, of course, subjective and may depend on driving style, street layout, or traffic density. However, the histogram in Fig. 6 suggests that time gaps below 2 s (i.e. approximately the first quartile of the distribution) are seldom observed and hence also should be avoided by an automated vehicle.

To realize an adequate system behavior we suggest that an automated vehicle monitors its future driving corridor, in particular with respect to violations of a defined minimum time gap. As illustrated in Fig. 7, we consequently define a comfort zone that extends along the vehicle's future path. The extent of the comfort zone reflects the time gap which is considered comfortable. In our implementation we choose a TTC of 3 s, which corresponds to a conservative driving style. The length of the comfort zone consequently depends on the vehicle's speed and thus can be adapted via braking (zone shrinks) or acceleration (zone is enlarged).

Furthermore, we propose that an automated vehicle evaluates whether its comfort zone is violated by a pedestrian – currently or in the future. This is done by predicting future pedestrian locations and intersecting them with the vehicle's future comfort zones (see Fig. 7a). The latter are derived by shifting the current comfort zone along the planned path assuming constant vehicle velocity (i.e. no change in system behavior). In case of violations, the automated vehicle issues a system reaction, e.g. braking, such that the pedestrian's future trajectory does not violate the adapted comfort zones anymore (see Fig. 7b).

From the above considerations it becomes evident that comfortable driving requires large prediction horizons. Pedestrians at least have to be predicted for a time horizon that corresponds to the comfort zone's time gap, i.e. 3 s in our case. To realize natural driving behavior even larger horizons are required such that future comfort zone violations can be anticipated. Requirements on prediction accuracy can be relaxed for larger prediction horizons as erroneous system reactions still can be corrected in the future. However, to minimize false system reactions it is required that behavior planning takes prediction uncertainties into account. Pedestrian prediction models hence should yield uncertainty estimates (e.g. in terms of probability distributions over future pedestrian locations).

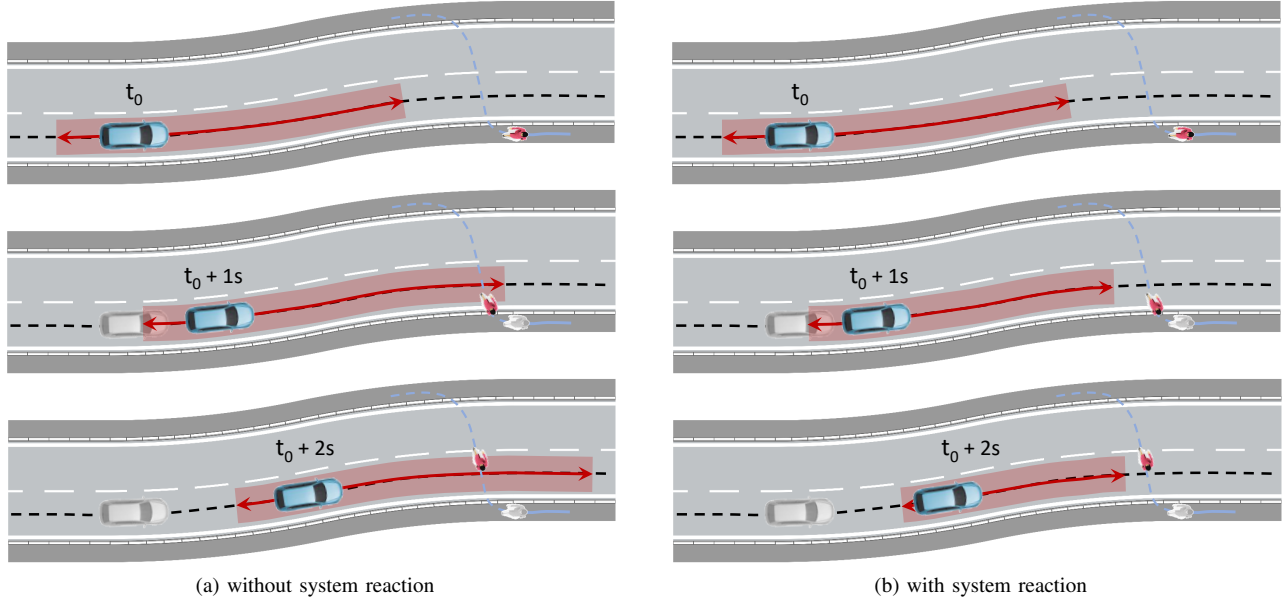


Fig. 7. Illustration of the proposed procedure to derive appropriate system reactions. In (a) the system first evaluates whether a pedestrian will violate the comfort zone in the future. In (b) a braking maneuver finally slows down the vehicle such that future comfort zone violations are circumvented. Dashed lines depict the paths of the vehicle and the pedestrian. The red regions corresponds to the vehicle's comfort zone.

It should be noted that the comfort zone is not necessarily restricted to regions in front of the vehicle. Rather, it may also cover a region behind the vehicle. This allows to evaluate whether the vehicle can pass a pedestrian with a sufficient time gap before the pedestrian enters the driving corridor. Similarly, the comfort zone may be extended to include infrastructure elements (e.g. zebra crossings as depicted in Fig. 8) such that country-specific traffic rules are taken into account.

### C. Prediction Performance Metric

Building on the AD system reaction we now derive an application specific performance metric for our prediction model. To this end we define pedestrian behavior prediction as a binary classification task.

Fig. 8a shows a typical traffic scene with the trajectory of a crossing pedestrian as well as the ego vehicle's comfort zone. The latter is referred to as region of interest (ROI) in the following. The task of a pedestrian prediction is to anticipate violations of the ROI, i.e. a classification whether a pedestrian will be located inside the ROI in the future. We define the in-ROI probability  $P_{t+T}^{\text{ROI}}$  at time  $t + T$  as

$$P_{t+T}^{\text{ROI}} = \int_{x_{t+T} \in \text{ROI}_{t+T}} p(x_{t+T} | x_{0:t}, C) dx_{t+T}, \quad (1)$$

where  $\text{ROI}_{t+T}$  denotes the predicted ROI and  $p(x_{t+T} | x_{0:t}, C)$  the predictive distribution of pedestrian locations given the pedestrian's past trajectory  $x_{0:t}$  and contextual cues  $C$ . Computing the in-ROI probability requires integration of the predictive distribution over the ROI. This is approximated with a Monte-Carlo approach using samples from the distribution.

Fig. 8b illustrates the evolvement of the scene and the prediction over time. Specifically, the dashed line represents the true state of the pedestrian with regard to being inside

the ROI for, say,  $T = 3$  s prediction horizons, whereas the solid blue line shows the predicted in-ROI probability for this prediction horizon. Thresholding  $P_{t+T}^{\text{ROI}}$  finally yields an in-ROI classification that is compared to the true state for each sample  $t$ .

Thus we have defined a classification problem (with pre-

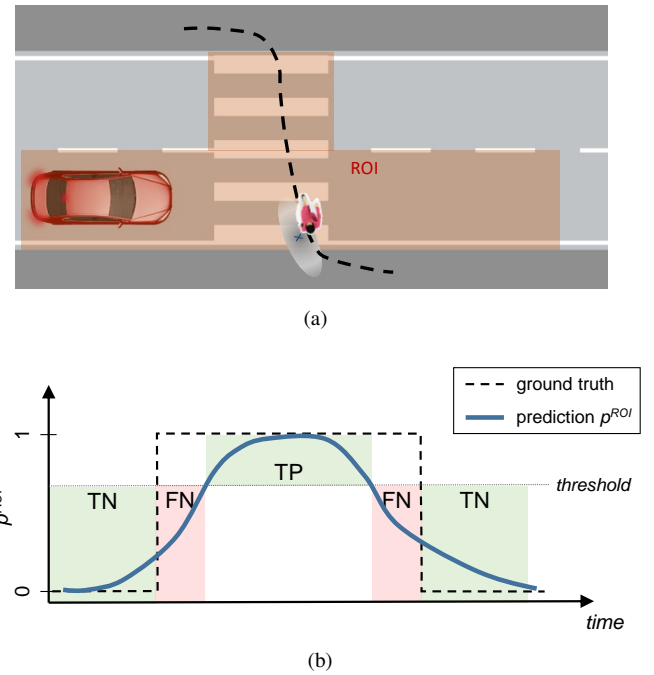


Fig. 8. Illustration of the proposed performance metric. (a) Ground truth pedestrian trajectory crossing the region of interest. (b) Prediction of in-ROI probability (solid) and ground truth of in-ROI state (dashed). For one recorded traffic scene, 3 s predictions of pedestrian and of ego vehicle ROI have been started from all possible points in time (x-axis).

dicted class probabilities) for which textbook metrics can be applied. In particular, we choose the true positive rate (TPR) and the false alarm rate (FAR) which are defined as

$$\text{TPR} = \text{TP}/(\text{TP} + \text{FN}) \quad (2)$$

$$\text{FAR} = \text{FP}/(\text{FP} + \text{TN}), \quad (3)$$

where TP, TN, FP, and FN denote number of true positive, true negative, false positive, and false negative samples, respectively. For metric calculation we accumulate classification results over the set of test tracks, but exclude samples at which a pedestrian has a TTC > 5s. This is in order to only consider predictions in the metric that could actually be relevant for an AD system decision. Moreover, we individually calculate the metric for different prediction time horizons, e.g.  $T \in \{1\text{ s}, 2\text{ s}, 3\text{ s}, 4\text{ s}\}$ .

It should be noted that the sensitivity of the classification can be adjusted by choosing different thresholds (see Fig. 8b). We consequently obtain an ROC curve which is appealing due to its intuitive interpretation. In particular, it allows for studying the trade off between TPR and FAR which would be difficult to define from requirements given a priori. A drawback of the ROC metric is that it can not be used as a per-track metric, because an individual pedestrian track contains too little data to result in a sufficient statistic.

That is why we additionally employ the log loss metric for development purposes. It can be computed per track so that studying the effect of model changes on the performance for specific tracks or kinds of traffic scenes is possible. On the downside, this metric does not have an intuitive function-level interpretation.

## V. PEDESTRIAN PREDICTION MODEL

Section IV analyzes human driving behavior and derives an expected AD system reaction pattern. Such a reaction pattern requires judging whether the probability of a pedestrian being inside a future comfort zone of the ego vehicle exceeds a certain threshold. Based on this reaction pattern, we can derive desired properties of prediction models:

- *Prediction of a continuous distribution over future pedestrian locations* for computing the likelihood of a pedestrian being inside the future comfort zone of the ego vehicle,
- *Predictive distributions over different prediction horizons* to evaluate comfort zone violations for different prediction horizons,
- *Ability to model complex multi-modal distributions* as future behavior can have several non-trivial modes (e.g. going straight or crossing the street),
- *Learning influences of the static and dynamic environment* that affect the pedestrians behavior.

In Section II, we refer to several recent approaches for pedestrian behavior prediction, which differ in terms of model types, architectures, learning method, or availability of features. However, most recent approaches use Deep Learning (DL) models for learning complex, non-linear functional dependencies from input features to the predicted behavior. Especially Conditional Variational Autoencoders (CVAEs) [16]

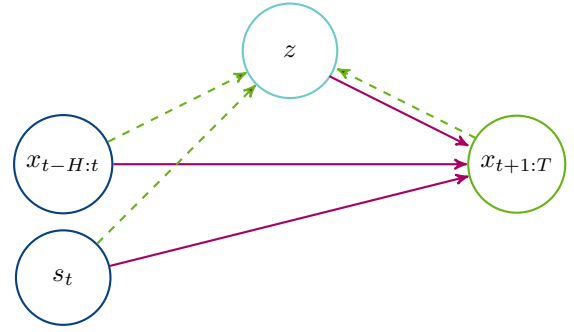


Fig. 9. CVAE with circles indicating random variables. Blue circles illustrate measurements of dynamic  $x_{t-H:t}$  and static features  $s_t$ , turquoise circles illustrate latent variables, and green circles represent predicted variables. Magenta arrows depict the prediction model, whereas green dashed arrows illustrate the inference model of the latent variable.

have proven to be suitable for such use cases as they can learn complex, continuous distributions by introducing continuous latent variables. Furthermore, they allow to incorporate feature observations by conditioning on them.

In this section, we introduce a model for pedestrian behavior prediction based on CVAEs and give an overview on architectures for learning dependencies of different types of features.

### A. General Model

Traditional DL-based probabilistic models often predict parameters of a pre-defined parametric distribution (e.g. Gaussian). However, for many problems the actual shape of the distribution is unknown and varies over situations. This fact makes it difficult to specify a suitable parametric distribution.

To overcome this problem, we propose a pedestrian prediction model based on a CVAE, which is depicted as a graphical model in Fig. 9. The circles represent different types of random variables: Blue circles correspond to measurements (the pedestrian trajectory including dynamic features  $x_{t-H:t}$  of the last  $H$  timesteps and a representation of the static environment  $s_t$ ), the turquoise circle is a continuous latent variable with prior  $p(z)$  (we stick to the Gaussian prior, which is used in many publications, e.g. [16]), and the green circle represents future pedestrian locations.

**Sampling:** The magenta arrows illustrate the sampling process of the induced predictive distribution:

- 1) Observe a pedestrian trajectory  $x_{t-H:t}$  and the environment around the pedestrian  $s_t$ .
- 2) Sample  $z$  from the Gaussian prior  $p(z) = N(z; 0, 1)$ .
- 3) Sample  $x_{t+1:T}$  from the conditional distribution  $p_\theta(x_{t+1:T}|x_{t-H:t}, s_t, z)$ .

Consequently, the predictive distribution of the CVAE (illustrated by magenta arrows), can be formulated as:

$$p_\theta(x_{t+1:T}|x_{t-H:t}, s_t) = \int_z p_\theta(x_{t+1:T}|x_{t-H:t}, s_t, z)p(z)dz. \quad (4)$$

We model  $p_\theta(x_{t+1:T}|x_{t-H:t}, s_t, z)$  by a multivariate normal distribution with parameters being predicted by a neural network. It should be emphasized however, that the predictive



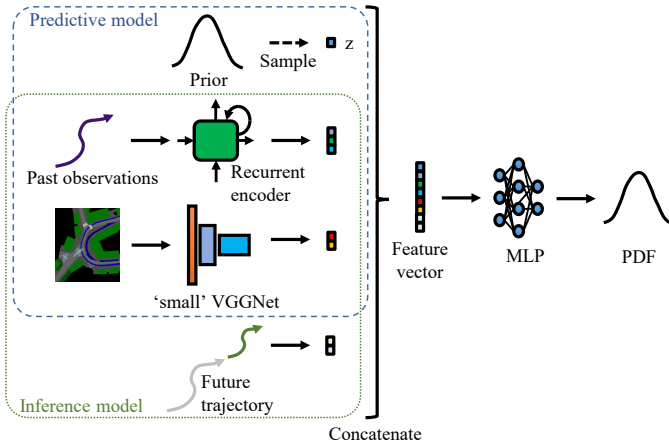


Fig. 10. DL-based architecture of the proposed CVAE. For inferring the latent variable, the inference model uses encoded past observations of a pedestrian, encoded static context of the environment, as well as the observed future trajectory. In contrast, the predictive model does not have access to the future trajectory, but predicts future locations given past observation, static context, and a sample of the latent variable  $z$ . The predictive and the inference model share the same encoders of past observations and static context.

distribution  $p_\theta(x_{t+1:T}|x_{t-H:t}, s_t)$  is not restricted to a multivariate Gaussian distribution but can be rather complex due to the integral over the latent variable  $z$ .

**Learning:** During training, the CVAE utilizes an inference model  $q_\phi(z|x_{t+1:T}, x_{t-H:t}, s_t)$  that infers a posterior distribution over the latent variable  $z$  from measurements and the observed future trajectory (green, dashed arrows in Fig. 9). We train the full model by minimizing the evidence lower bound (ELBO), which is a lower bound on the conditional log likelihood of the model in Eq. (4):

$$\mathbb{E}_{q_\phi(z|x_{t+1:T}, s_t)} [\log p_\theta(x_{t+1:T}|x_{t-H:t}, s_t, z)] - D_{KL}(q_\phi||p(z)) \quad (5)$$

The first term corresponds to a reconstruction loss as used for training autoencoders. Drawing on this analogy, we can consider the inference model  $q_\phi$  as encoder, that encodes past and future observations into the latent state  $z$ . Then, the distribution  $p_\theta$  corresponds to the decoder, which tries to reconstruct the future trajectory from the latent state. The latter term is the Kullback–Leibler divergence  $D_{KL}(q_\phi||p(z))$  between the posterior distribution  $q_\phi$  and the prior distribution  $p(z)$ . This term forces the inference model to match the uninformative Gaussian prior. Consequently, the first term tries to encode information into  $z$  and the latter term tries to prevent it. For  $q_\phi = p(z)$  the KL-term vanishes and no information is incorporated into  $z$ . In this case, the model does not make use of the latent space at all. However, this only happens if the conditional model  $p_\theta(x_{t+1:T}|x_{t-H:t}, s_t, z)$  is complex enough to model the data distribution without using  $z$ , e.g. all modeling assumptions are correct (model complexity, conditional Gaussian, etc.). This property of CVAEs enables an adaptive model complexity that proves useful if complexity varies over situations.

## B. Baseline model and feature integration

A CVAE allows for integrating features by conditioning on them. As indicated in Fig. 9 we propose to condition on both static information at a particular timestep  $s_t$  as well as dynamic information of the agents  $x_{0:t}$ . For conditioning on such information, we propose the DL-based architecture depicted in Fig. 10.

We encode dynamic features of the agent  $x_{t-H:t}$  (e.g. relative motion between two timesteps, head pose, body pose, distance to the ego vehicle) via recurrent encoders into an embedding space. In addition, we represent the static environment around the pedestrian via a grid in birds eye view, where different colors indicate different semantics (e.g. sidewalk, road, zebra crossing, building, isle, bicycle lane, unknown). These birds eye view grids are encoded via a small VGGNet architecture to provide a static environment embedding vector.

**Predictive model**  $p_\theta(x_{t+1:T}|x_{t-H:t}, s_t, z)$  (**dashed blue rectangle**): For the predictive model, the static environment embedding, the dynamic environment embedding, as well as a sample  $z$  from the  $Z$ -dimensional multivariate Gaussian prior  $p(z)$  are concatenated together to form a feature vector. This feature vector is transformed via an MLP to generate parameters of a joint distribution over the future pedestrian locations in  $x$  and  $y$  at four prediction timesteps (1s, 2s, 3s, 4s). We model the joint output distribution as an 8-dimensional Gaussian distribution.

**Inference model**  $q_\phi(z|x_{t+1:T}, x_{t-H:t}, s_t)$  (**dotted green rectangle**): The inference model  $q_\phi$  infers the latent variable  $z$  that has created the observed future. As input the corresponding inference model receives the static environment embedding, the dynamic environment embedding of the past, and the relative future motion of the pedestrian, which are concatenated into one joint feature vector. Then an MLP is used to transform this feature vector into a  $Z$ -dimensional Gaussian distribution.

**Feature combinations:** The proposed architecture allows for flexible changes of input features and enables an ablation study regarding the influence of different features on the prediction performance. Table I denotes the features that we have evaluated in this study. The most basic model only conditions on the past motion of the pedestrian and does not use any additional information. Hence, it can only learn future predictions based on cues in the pedestrian trajectory itself.

TABLE I  
DESCRIPTION OF FEATURES USED IN THE CVAE.

Feature	Description
Motion	Pedestrian relative motion (dx, dy) at every timestep.
Ego	Distance between pedestrian and ego vehicle at every timestep.
Head	Head pose of the pedestrian at every timestep.
Body	Body pose of the pedestrian at every timestep.
Map	Semantic map around the last position of the pedestrian.

## VI. EXPERIMENTAL RESULTS

### A. Experimental Setup

Training, validation and test subsets are drawn from three round courses in our dataset. The fourth course is reserved for

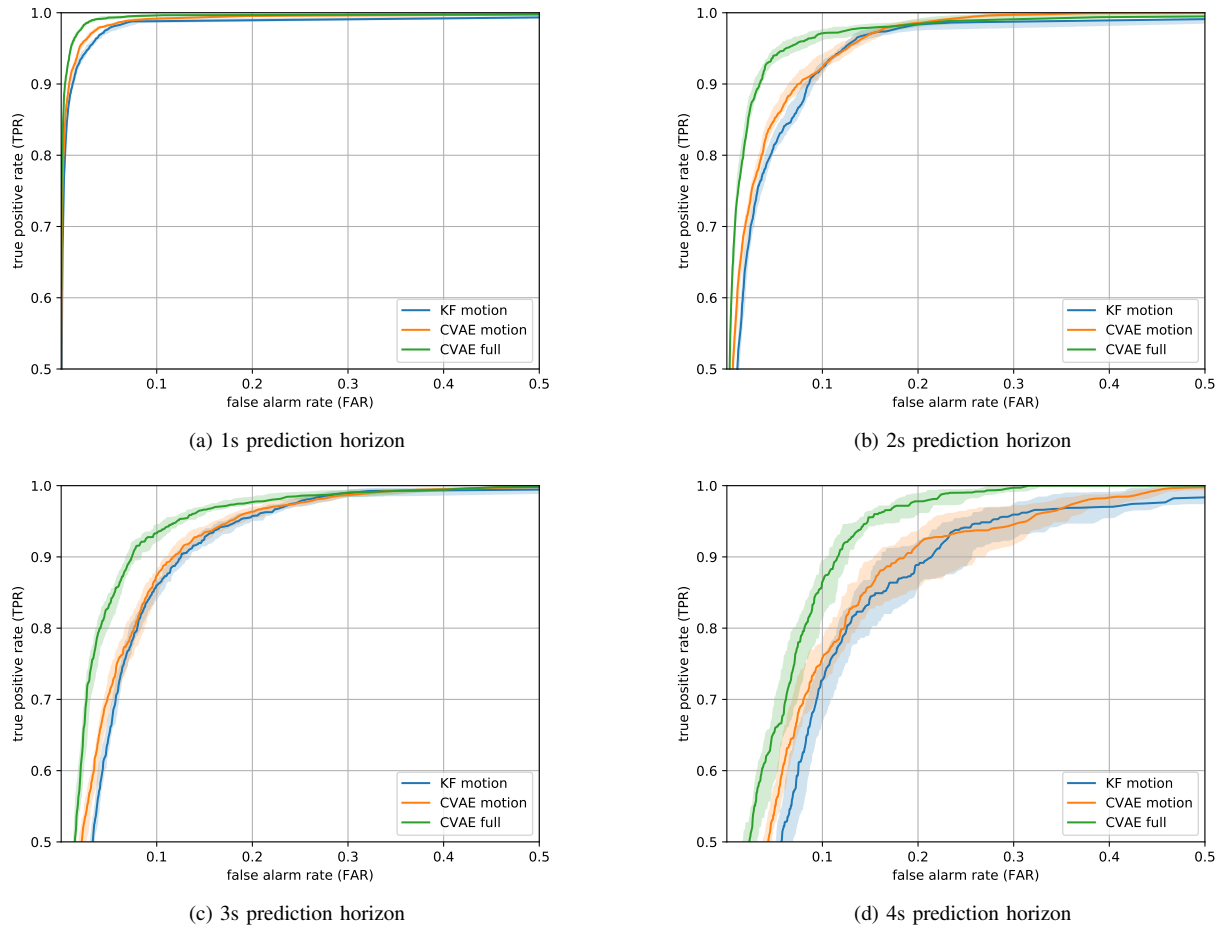


Fig. 11. ROI-based metric results of the full CVAE model (all features), a CVAE motion model (pedestrian motion feature only) and a linear Kalman Filter baseline for different prediction horizons. The shaded bands denote the inter quartile interval per FAR.

studying the effects of areas not exposed to the model during training. The dataset is split by first assembling the test set. In order to be able to evaluate how pedestrian features like head pose affect the prediction performance, the whole test set needs to consist of labeled tracks. With the fraction of labeled tracks in the dataset being comparatively small, the test set has to be limited in size to ensure enough labeled tracks are available for training. We decided to constrain the test set size to 500 tracks while at the same time guaranteeing a large variety of scenes. This is achieved by drawing from the labeled subset via stratified random sampling, with each category, e.g. crossing/not crossing, distance from ego vehicle, crossing in front/behind the ego vehicle, being represented at least once.

For training and validation, a minimum track length of 5s is required to enable training of prediction horizons of up to 4s. 5% of the tracks fulfilling this criterion are randomly assigned to the validation set, the remaining tracks form the training set. Training and validation set contain 42,551 (7,175 labeled) and 2,278 (389 labeled), respectively.

### B. Quantitative Evaluation

To benchmark the performance of the proposed CVAE prediction model, we compare against a linear baseline that

employs Kalman Filtering (KF) using a constant velocity model (*KF motion*). We provide results for a CVAE model that solely uses a pedestrian’s past trajectory (*CVAE motion*) as well as a CVAE model that employs a full feature set (*CVAE full*) consisting of the pedestrian’s past trajectory, their head and body poses, the semantic map and the past ego vehicle’s trajectory. In this way the effect of contextual cues on the prediction performance can be assessed. We run all three models on the test dataset and evaluate the predictions using the application-specific ROI-metric proposed in Sec. IV-C.

In order to assess the variance of the test results, evaluations are repeated using the bootstrap method [42] with  $B = 20$  replications. Each replication uses an artificial test set created from the original test set by resampling 500 tracks with replacement. The bootstrap method produces an estimate of the variance that would be seen with completely new test data taken from the same ground truth distribution of data.

The resulting ROC curves for different prediction horizons are depicted in Fig. 11 (solid line: median TPR per FAR, shaded area: inter quartile interval per FAR). It becomes evident that the prediction accuracies of all models decrease with increasing prediction horizons. For a prediction horizon of 1s all models achieve very good accuracies with the CVAE models slightly outperforming the linear KF baseline. This

TABLE II  
PERFORMANCE OF PEDESTRIAN PREDICTION MODELS

Model	ROI True Positive Rate (%)				Negative Log-Likelihood				ADE (m)			
	1s	2s	3s	4s	1s	2s	3s	4s	1s	2s	3s	4s
KF motion	94.3	81.5	86.0	84.1	2.40	3.96	4.89	5.47	0.62	1.26	1.99	2.87
CVAE motion	96.1	85.1	87.4	85.8	0.23	1.63	2.47	3.23	0.54	1.13	1.77	2.58
CVAE full	<b>98.3</b>	<b>94.0</b>	<b>93.3</b>	<b>95.5</b>	<b>-0.20</b>	<b>1.11</b>	<b>1.95</b>	<b>2.72</b>	<b>0.47</b>	<b>0.96</b>	<b>1.50</b>	<b>2.23</b>

result confirms that for short-term pedestrian prediction linear prediction models are already well suited and that contextual cues only have a minor benefit. However, the contrary holds for prediction horizons of 2 to 4s. While the CVAE motion model just slightly surpasses the KF baseline, the full CVAE model significantly outperforms it. Our results thus confirm the importance of using contextual cues for long-term pedestrian prediction.

For an application of prediction models in an AD system, the performance at low FAR is of particular interest, since high FAR would result in an unacceptable number of false system reactions. However, acceptable FARs differ with respect to prediction horizons – larger prediction horizons usually correspond to less critical situations so that there is sufficient time left to correct potential erroneous system reactions. We hence allow for slightly larger FARs for long-term prediction compared to very small FARs in the short-term prediction case. Specifically, we consider FARs of 2.5%, 5%, 10%, and 15% as suitable working points for the 1s, 2s, 3s, and 4s prediction models, respectively. The corresponding TPRs of the three models are listed in Table II.

Table II further lists the respective values for the negative log-likelihood and the ADE metric. We show ADE here because it gives an impression of the order of magnitude of the model error in terms of physical dimensions (meters). The results reveal that the ADE values are quite strongly correlated with the negative log-likelihood values in this case, which is in contrast to our earlier statement about the applicability of ADE to multimodal predictions (see Section II-C). Analysing model predictions more closely as will be done in Section VI-D, we notice that most model predictions are unimodal. We attribute this to multimodal behavior being underrepresented in the training data.

### C. Feature Relevance Assessment

To analyze the relevance of different contextual cues we performed an ablation study whose results are shown in Table III. We list the true positive rate (TPR) and the negative log-likelihood (NLL) for CVAE models that use different input feature combinations, respectively. Numbers in large font are medians from the bootstrap analysis, while small font numbers indicate inter quartile ranges (25% and 75% quartile).

As expected, the consideration of contextual cues positively influence model performance compared to the baseline CVAE motion model, in particular for larger prediction time horizons. This is in accordance with Fig. 11 and consistent across almost all model variants. Subtle deviations from this general trend will be discussed later in this section.

Furthermore, it is obvious that the map is crucial for good prediction performance, when comparing models 1-4 (without map) to models 5-8 (with map). The positive effect of using a map is particularly pronounced for prediction horizons of 2s to 4s. Checking the interquartile intervals of the corresponding models with and without map, we see that they are non-overlapping in most cases. This gives us confidence that the differences in model performance are significant.

The 2s to 4s predictions with map further indicate that adding either ego or head+body feature slightly improves performance (models 6 and 7 compared to model 5). However, the interquartile intervals for models 6 and 7 overlap strongly with the intervals for model 5 in most cases. Instead, including both features, i.e. ego+head+body, yields significantly better results. This shows that the combination of them contains valuable information. The same trend can be observed for the set of models without map.

A notable exception to this general trend can be observed for the ego feature (models 2 and 6), where the TPR deteriorates for 3s and 4s prediction horizons. Interestingly, this effect cannot be observed in NLL. Even though the effect is not significant as the interquartile intervals strongly overlap, it is still surprising that adding ego does tamper with the median TPR. This might be caused by the metrics measuring different aspects of model performance, while the training objective is more correlated to NLL than to the ROI metric. The investigation of more system-centric training objectives could thus be a promising field of future research.

### D. Qualitative Evaluation

The feature relevance assessment in Section VI-C indicates that CVAE-based models with additional features can significantly outperform the baseline. In the following, we provide qualitative examples, which highlight the influence of features on pedestrian prediction using our proposed CVAE-based model. Fig. 12 illustrates two scenes that often occur in urban scenarios. In the first scene, Fig. 12a and 12b, a pedestrian is walking on the sidewalk (dark gray) parallel to the street (light gray) and approaching a zebra crossing (violet). The CVAE motion model in Fig. 12a does not have information about the static environment and thus mainly predicts straight walking with some uncertainty. Instead, the CVAE with map feature in Fig. 12b was able to learn that zebra crossings increase likelihoods of pedestrians to cross and it correctly skews the distribution towards the zebra crossing, while still keeping a mode for straight walking. The second scene, Fig. 12c and 12d, shows a pedestrian that stands at the side of a street and waits for crossing, while a car is decelerating to let the pedestrian pass. The CVAE motion



TABLE III  
ABLATION STUDY OF CONTEXTUAL CUES

Model	ROI True Positive Rate (%)								Negative Log-Likelihood							
	1 s		2 s		3 s		4 s		1 s		2 s		3 s		4 s	
1 CVAE motion	96.1	96.3 95.6	85.1	86.9 84.0	87.4	88.4 84.6	85.8	89.6 82.7	0.23	0.20 0.25	1.63	1.60 1.68	2.47	2.44 2.55	3.23	3.19 3.32
2 CVAE motion+ego	97.2	97.6 96.6	88.0	89.1 87.1	89.7	91.2 88.6	84.4	90.5 81.4	-0.10	-0.12 -0.07	1.32	1.28 1.38	2.20	2.15 2.26	3.05	2.98 3.14
3 CVAE motion+head+body	97.3	97.8 96.8	89.5	91.2 88.6	89.3	91.2 88.0	86.1	90.9 82.1	0.13	0.11 0.15	1.54	1.52 1.59	2.40	2.37 2.48	3.18	3.13 3.26
4 CVAE motion+ego+head+body	97.9	98.3 97.6	91.8	93.1 90.8	91.5	92.4 90.2	88.0	92.2 84.9	-0.12	-0.16 -0.10	1.29	1.25 1.34	2.16	2.11 2.24	2.97	2.89 3.05
5 CVAE motion+map	97.7	98.4 97.4	91.2	92.5 90.3	91.6	93.1 89.8	92.8	94.4 90.0	0.04	0.01 0.05	1.35	1.31 1.38	2.14	2.10 2.21	2.86	2.79 2.95
6 CVAE motion+map+ego	97.9	98.2 97.3	92.7	94.0 92.2	91.4	92.8 89.9	91.0	91.6 87.9	-0.17	-0.20 -0.15	1.17	1.14 1.21	1.99	1.95 2.06	2.79	2.71 2.87
7 CVAE motion+map+head+body	97.9	98.4 97.6	92.6	93.6 91.3	92.9	93.4 92.0	94.6	96.2 91.6	-0.02	-0.03 0.00	1.29	1.26 1.33	2.08	2.04 2.14	2.80	2.74 2.91
8 CVAE motion+map+ego+head+body	<b>98.3</b>	98.7 98.1	<b>94.0</b>	94.9 92.9	<b>93.3</b>	94.5 92.1	<b>95.5</b>	96.5 94.3	<b>-0.20</b>	-0.23 -0.18	<b>1.11</b>	1.08 1.14	<b>1.95</b>	1.91 2.02	<b>2.72</b>	2.65 2.82

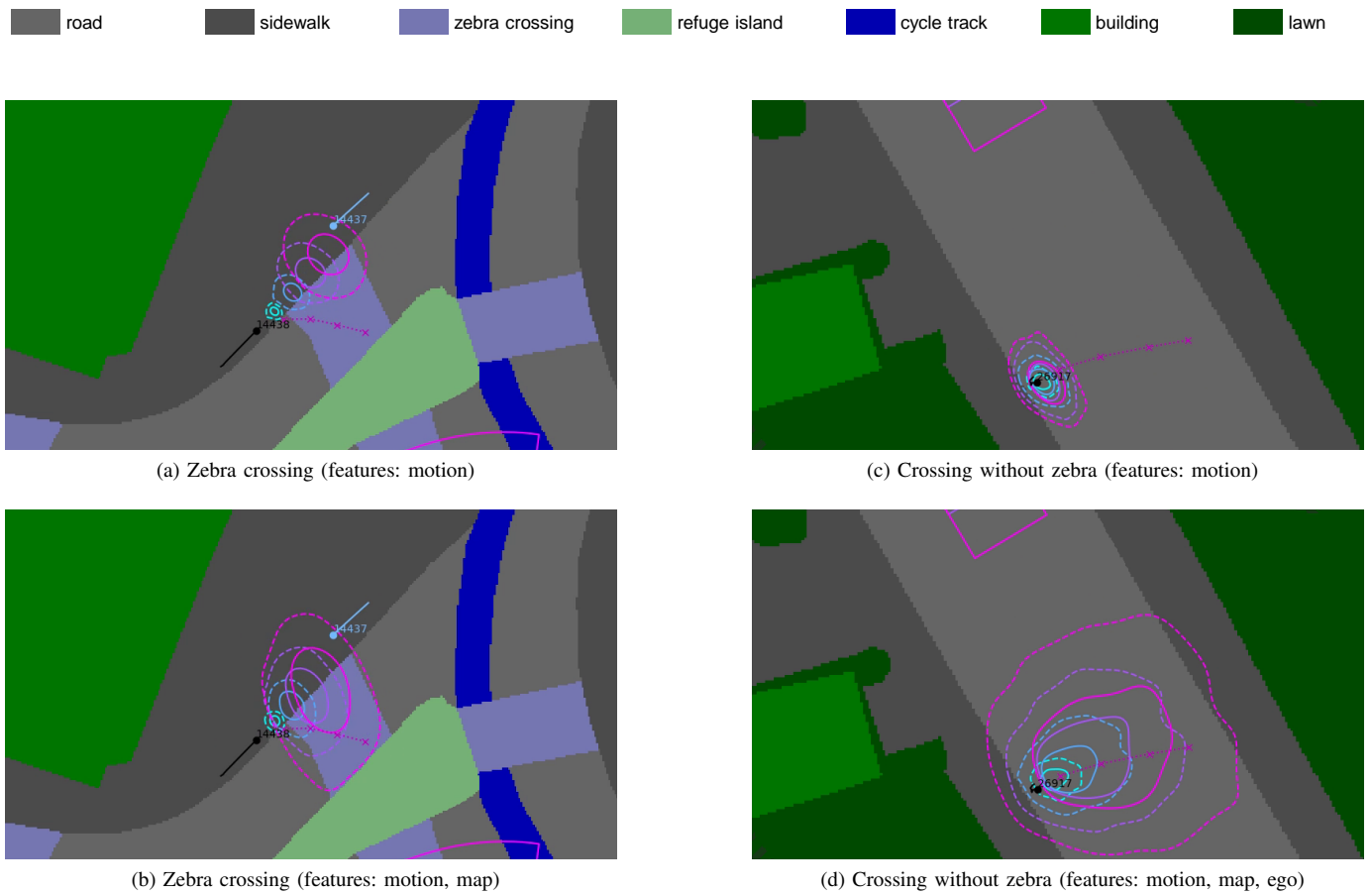


Fig. 12. Pedestrian behavior prediction of the proposed model in two different scenarios. The circles indicate predictions for 1s (turquoise), 2s (blue), 3s (purple), and 4s (magenta), while the dashed line with crosses indicate the groundtruth future trajectory. In the first scenario, depicted in (a) and (b), a pedestrian is walking towards a zebra crossing after walking straight on the sidewalk, but parallel to the street. In the second scenario, depicted in (c) and (d), a pedestrian is starting to cross the street without a zebra crossing, after a car has reduced its speed (prediction of the car is illustrated by a magenta box at the top).

model in Fig. 12c with only pedestrian features is not able to predict that the likelihood increases for the pedestrian to start walking, while the CVAE model with map and ego vehicle features in Fig. 12d picks up this information very fast and predicts the pedestrian to cross the street.

## VII. CONCLUSION

With the shift from advanced driver assistance systems towards fully automated driving, novel requirements on pedestrian behavior prediction arise. In this paper we argued that these requirements are not fully taken into account by established evaluation procedures – particularly in terms of metrics and datasets that are usually used to quantitatively assess pre-

diction performance. We proposed a system-level approach to bridge this gap: Based on a large dataset comprising thousands of pedestrian-vehicle interactions, we analyzed human driving patterns, designed corresponding reaction patterns of an AD system, and finally derived respective requirements on a pedestrian behavior prediction component. Moreover, we proposed a novel evaluation metric that measures the fulfillment of these requirements and hence eases a system-level interpretation of results. Our contribution thus shall stimulate future research on system-level evaluation and optimization of prediction models.

We additionally proposed a CVAE-based model for pedestrian behavior prediction that allows for a flexible integration of additional contextual cues. Using this model, we demonstrated the importance of using scene context – particularly for long-term prediction horizons that are of utmost importance for AD systems. A thorough ablation study shed light on the relative importance of different features. To this end we conclude that all investigated features aid the prediction task, but to different extents: A semantic map most notably contributes to an improved long-term prediction performance, whereas a pedestrian’s head and body orientation yield positive effects at smaller prediction horizons. Best results were obtained by a combination of all features.

Our future work will focus on the integration and optimization of the developed prediction component in an AD system. Furthermore, we will investigate the relevance of additional contextual features.

## VIII. ACKNOWLEDGMENTS

This work is a result of the research project @CITY-AF — Automated Cars and Intelligent Traffic in the City: Automated Driving Functions. The project is supported by the Federal Ministry for Economic Affairs and Energy (BMWi), based on a decision taken by the German Bundestag. The authors are solely responsible for the content of this publication.

## APPENDIX A IMPLEMENTATION DETAILS

### A. Model Architecture

**Recurrent encoder:** We compute an embedding of the observed pedestrian trajectory  $x_{t-H:t}$  using a recurrent encoder. This encoder consists of two stacked Long Short-Term Memory (LSTM) cells producing a 128 dimensional embedding vector. Both cells use the same state size which is determined for each input feature combination by means of a hyperparameter search. The observation horizon  $H$  is set to 10 time steps, which corresponds to one second.

**Map encoder:** The static environment, represented as a birds eye view semantic grid, is encoded via a small Convolutional Neural Network (CNN). The CNN processes grids of size  $256 \times 256$  pixels, containing the agent’s local environment of size  $25.6 \text{ m} \times 25.6 \text{ m}$  centered around the position of the pedestrian at the last conditioning time step. The architecture of the CNN is defined by the shortcut notation:

$$C'_4-P-C'_8-P-C'_{16}-C'_{16}-P-C'_{32}-C'_{32}-P-C'_{64}-C'_{64}-P-F'_{512}-F_{100},$$

where  $C_i$  is a convolutional layer with  $i$  filters, a stride of 1 and a filter size of  $3 \times 3$ ,  $P$  a max-pooling layer with non-overlapping  $2 \times 2$  regions and  $F_i$  a fully connected layer with  $i$  output features. A prime marks layers which apply a ReLU nonlinearity.

**Feature transformers:** The predictive model and the inference model each use a Multilayer Perceptron (MLP) to transform feature vectors to parameters of a n-dimensional Gaussian distribution. The dimensionality  $n$  is set to 8 for the predictive model and to 10 for the inference model. Both MLPs consist of 3 fully connected layers and utilize ReLU nonlinearities. The number of output features is identical in each layer and derived using a hyperparameter search. Missing features are replaced by a constant value of 0.

### B. Model training

We perform a grid search to determine for each input feature combination the best model. The parameters of our hyperparameter search space are listed in Table IV. In total, we train 60 models for each input feature combination and pick the best model based on the validation hitrate. Models are trained for 3000 epochs using the Adam optimizer and a learning rate of 0.001. To augment the training data, we randomly rotate the trajectories and environment maps.

	Models with map	Models without map
State size of LSTM cells	256, 384	256, 384
Features per MLP layer	256, 384, 512	384, 512, 640
Random seeds	1, ..., 10	1, ..., 10

TABLE IV

HYPERPARAMETER SEARCH SPACE.

## REFERENCES

- [1] *Global status report on road safety 2018*. Geneva: World Health Organization, 2018.
- [2] S. H. Haus, R. Sherony, and H. C. Gabler, “Estimated benefit of automated emergency braking systems for vehicle–pedestrian crashes in the United States,” *Traffic Injury Prevention*, vol. 20, no. Suppl. 1, pp. S171–S176, 2019. [Online]. Available: <https://doi.org/10.1080/15389588.2019.1602729>
- [3] A. Rudenko, L. Palmieri, M. Herman, K. M. Kitani, D. M. Gavrila, and K. O. Arras, “Human motion trajectory prediction: A survey,” 2019.
- [4] E. Mazor, A. Averbuch, Y. Bar-Shalom, and J. Dayan, “Interacting multiple model methods in target tracking: a survey,” *IEEE Transactions on aerospace and electronic systems*, vol. 34, no. 1, pp. 103–123, 1998.
- [5] T. Gindele, S. Brechtel, and R. Dillmann, “A probabilistic model for estimating driver behaviors and vehicle trajectories in traffic environments,” in *Proceedings of the IEEE International Conference on Intelligent Transportation Systems (ITSC)*, 2010, pp. 1625–1631.
- [6] G. Agamennoni, J. I. Nieto, and E. M. Nebot, “Estimation of multivehicle dynamics by considering contextual information,” *IEEE Transaction on Robotics (TRO)*, vol. 28, no. 4, pp. 855–870, 2012.
- [7] A. Alahi, K. Goel, V. Ramanathan, A. Robicquet, L. Fei-Fei, and S. Savarese, “Social LSTM: Human trajectory prediction in crowded spaces,” in *Proceedings of the IEEE Conference on Computer Vision and Pattern Recognition (CVPR)*, 2016, pp. 961–971.
- [8] E. Zhan, S. Zheng, Y. Yue, and P. Lucey, “Generative multi-agent behavioral cloning,” *arXiv:1803.07612*, 2018.
- [9] N. Deo and M. M. Trivedi, “Multi-modal trajectory prediction of surrounding vehicles with maneuver based LSTMs,” in *Proceedings of the IEEE Intelligent Vehicle Symposium (IV)*, 2018, pp. 1179–1184.
- [10] Y. Chai, B. Sapp, M. Bansal, and D. Anguelov, “Multipath: Multiple probabilistic anchor trajectory hypotheses for behavior prediction,” in *Conference on Robot Learning*, 2020, pp. 86–99.

- [11] A. Kuefler, J. Morton, T. Wheeler, and M. Kochenderfer, "Imitating driver behavior with generative adversarial networks," in *2017 IEEE Intelligent Vehicles Symposium (IV)*. IEEE, 2017, pp. 204–211.
- [12] C. Tang and R. R. Salakhutdinov, "Multiple futures prediction," in *Advances in Neural Information Processing Systems*, 2019, pp. 15424–15434.
- [13] N. Lee, W. Choi, P. Vernaza, C. B. Choy, P. H. Torr, and M. Chandraker, "Desire: Distant future prediction in dynamic scenes with interacting agents," in *Proceedings of the IEEE Conference on Computer Vision and Pattern Recognition*, 2017, pp. 336–345.
- [14] P. Felsen, P. Lucey, and S. Ganguly, "Where will they go? predicting fine-grained adversarial multi-agent motion using conditional variational autoencoders," in *Proceedings of the European Conference on Computer Vision (ECCV)*, 2018, pp. 732–747.
- [15] A. Bhattacharyya, M. Hanselmann, M. Fritz, B. Schiele, and C.-N. Straehle, "Conditional flow variational autoencoders for structured sequence prediction," in *Bayesian Deep Learning NeurIPS 2019 Workshop*, 2019.
- [16] K. Sohn, H. Lee, and X. Yan, "Learning structured output representation using deep conditional generative models," in *Advances in neural information processing systems*, 2015, pp. 3483–3491.
- [17] J. F. P. Kooij, N. Schneider, F. Flohr, and D. M. Gavrila, "Context-based pedestrian path prediction," in *Computer Vision – ECCV 2014*, D. Fleet, T. Pajdla, B. Schiele, and T. Tuytelaars, Eds. Cham: Springer International Publishing, 2014, pp. 618–633.
- [18] W.-C. Ma, D.-A. Huang, N. Lee, and K. M. Kitani, "Forecasting interactive dynamics of pedestrians with fictitious play," in *Proceedings of the IEEE Conference on Computer Vision and Pattern Recognition (CVPR)*, July 2017.
- [19] A. Elnagar and K. Gupta, "Motion prediction of moving objects based on autoregressive model," *IEEE Transactions on Systems, Man, and Cybernetics - Part A: Systems and Humans*, vol. 28, no. 6, pp. 803–810, 1998.
- [20] M. Bénéwitz, W. Burgard, G. Cielniak, and S. Thrun, "Learning motion patterns of people for compliant robot motion," *The International Journal of Robotics Research*, vol. 24, no. 1, pp. 31–48, 2005.
- [21] C. Schöller, V. Aravantinos, F. Lay, and A. Knoll, "What the constant velocity model can teach us about pedestrian motion prediction," *IEEE Robotics and Automation Letters*, vol. 5, no. 2, pp. 1696–1703, 2020.
- [22] P. Trautman and A. Krause, "Unfreezing the robot: Navigation in dense, interacting crowds," in *2010 IEEE/RSJ International Conference on Intelligent Robots and Systems*, 2010, pp. 797–803.
- [23] M. Kuderer, H. Kretschmar, C. Sprunk, and W. Burgard, "Feature-based prediction of trajectories for socially compliant navigation," in *Proc. of Robotics: Science and Systems (RSS)*, Sydney, Australia, July 2012.
- [24] A. Robicquet, A. Sadeghian, A. Alahi, and S. Savarese, "Learning social etiquette: Human trajectory prediction in crowded scenes," in *European Conference on Computer Vision (ECCV)*, 2016, pp. 549–565.
- [25] N. Schneider and D. M. Gavrila, "Pedestrian path prediction with recursive bayesian filters: A comparative study," in *German Conference on Pattern Recognition*. Springer, 2013, pp. 174–183.
- [26] M. Luber, L. Spinello, J. Silva, and K. O. Arras, "Socially-aware robot navigation: A learning approach," in *2012 IEEE/RSJ International Conference on Intelligent Robots and Systems*. IEEE, 2012, pp. 902–907.
- [27] F. Bartoli, G. Lisanti, L. Ballan, and A. Del Bimbo, "Context-aware trajectory prediction," in *2018 24th International Conference on Pattern Recognition (ICPR)*. IEEE, 2018, pp. 1941–1946.
- [28] C. Tang and R. R. Salakhutdinov, "Multiple futures prediction," in *Advances in Neural Information Processing Systems*, 2019, pp. 15424–15434.
- [29] J. Gao, C. Sun, H. Zhao, Y. Shen, D. Anguelov, C. Li, and C. Schmid, "Vectornet: Encoding hd maps and agent dynamics from vectorized representation," in *Proceedings of the IEEE/CVF Conference on Computer Vision and Pattern Recognition*, 2020, pp. 11525–11533.
- [30] L. Theis, A. van den Oord, and M. Bethge, "A note on the evaluation of generative models," in *International Conference on Learning Representations*, 2016, arXiv:1511.01844. [Online]. Available: <http://arxiv.org/abs/1511.01844>
- [31] B. Völz, K. Behrendt, H. Mielenz, I. Gilitschenski, R. Siegwart, and J. Nieto, "A data-driven approach for pedestrian intention estimation," in *2016 IEEE 19th International Conference on Intelligent Transportation Systems (ITSC)*, 2016, pp. 2607–2612.
- [32] W. J. Youden, "Index for rating diagnostic tests," *Cancer*, vol. 3, no. 1, pp. 32–35, 1950.
- [33] K. P. Murphy, *Machine Learning: A Probabilistic Perspective*. The MIT Press, 2012.
- [34] A. Rasouli, I. Kotseruba, and J. K. Tsotsos, "Are they going to cross? a benchmark dataset and baseline for pedestrian crosswalk behavior," in *2017 IEEE International Conference on Computer Vision Workshops (ICCVW)*, 2017, pp. 206–213.
- [35] A. Rasouli, I. Kotseruba, T. Kunic, and J. Tsotsos, "Pie: A large-scale dataset and models for pedestrian intention estimation and trajectory prediction," in *2019 IEEE/CVF International Conference on Computer Vision (ICCV)*, 2019, pp. 6261–6270.
- [36] J. F. P. Kooij, N. Schneider, F. Flohr, and D. M. Gavrila, "Context-based pedestrian path prediction," in *Computer Vision – ECCV 2014*, D. Fleet, T. Pajdla, B. Schiele, and T. Tuytelaars, Eds. Springer International Publishing, 2014, pp. 618–633.
- [37] S. Pellegrini, A. Ess, K. Schindler, and L. van Gool, "You'll never walk alone: Modeling social behavior for multi-target tracking," in *2009 IEEE 12th International Conference on Computer Vision*, 2009, pp. 261–268.
- [38] M.-F. Chang, J. Lambert, P. Sangkloy, J. Singh, S. Bak, A. Hartnett, D. Wang, P. Carr, S. Lucey, D. Ramanan, and J. Hays, "Argoverse: 3d tracking and forecasting with rich maps," in *Proceedings of the IEEE/CVF Conference on Computer Vision and Pattern Recognition (CVPR)*, June 2019.
- [39] P. Sun, H. Kretschmar, X. Dotiwala, A. Chouard, V. Patnaik, P. Tsui, J. Guo, Y. Zhou, Y. Chai, B. Caine, V. Vasudevan, W. Han, J. Ngiam, H. Zhao, A. Timofeev, S. Ettinger, M. Krivokon, A. Gao, A. Joshi, Y. Zhang, J. Shlens, Z. Chen, and D. Anguelov, "Scalability in perception for autonomous driving: Waymo open dataset," in *Proceedings of the IEEE/CVF Conference on Computer Vision and Pattern Recognition (CVPR)*, June 2020.
- [40] H. Caesar, V. Bankiti, A. H. Lang, S. Vora, V. E. Liong, Q. Xu, A. Krishnan, Y. Pan, G. Baldan, and O. Beijbom, "nusenes: A multi-modal dataset for autonomous driving," in *Proceedings of the IEEE/CVF Conference on Computer Vision and Pattern Recognition (CVPR)*, June 2020.
- [41] W. Zhan, L. Sun, D. Wang, H. Shi, A. Clause, M. Naumann, J. Kümmerle, H. Königshof, C. Stiller, A. de La Fortelle, and M. Tomizuka, "INTERACTION Dataset: An INTERNATIONAL, Adversarial and Cooperative MOTION Dataset in Interactive Driving Scenarios with Semantic Maps," *arXiv:1910.03088 [cs, eess]*, 2019.
- [42] B. Efron and R. J. Tibshirani, *An Introduction to the Bootstrap*, ser. Mono. Stat. Appl. Probab. London: Chapman and Hall, 1993. [Online]. Available: <https://cds.cern.ch/record/526679>



**Michael Herman** is a research scientist and sub-project lead at the Bosch Center for Artificial Intelligence working on machine learning-based motion prediction for automated driving. He received his Ph.D. degree in computer science from the University of Freiburg in an industrial Ph.D. program, where his research focused on learning generalizable representations of an experts motivations from observed behavior in complex, unknown environments. His current research is focused on learning prediction models in multi-agent systems with a focus on automated driving use cases, while his research interests include Probabilistic Inference, Deep Learning, and Imitation Learning.



**Jörg Wagner** received his M.Sc degree in electrical engineering and information technology from the Karlsruhe Institute of Technology, Germany, in 2014. He is a research engineer at Bosch Center for Artificial Intelligence (BCAI) working on machine learning-based motion prediction for automated driving. While working at BCAI, he is currently pursuing the Ph.D. degree with the University of Bonn, Germany. His research interests include deep learning, interpretable and explainable AI, computer vision and time series modeling.





**Vishnu Prabhakaran** received his M.Sc degree in Information Technology in 2018 from the University of Stuttgart, Germany, with a focus on machine learning and robotics. He is a research engineer at Bosch Center for Artificial Intelligence, working on multi-agent behavior prediction models for automated driving. His research interests include probabilistic inference, deep learning and time series modeling.



**Ernst Kloppenburg** received his Dr.-Ing. (Ph.D.) degree from University of Stuttgart in 1999 in Technical Cybernetics / Control Engineering. He is a senior expert at Bosch Center for Artificial Intelligence, working in the fields of probabilistic inference, and of verification of machine learning systems.



**Nicolas Möser** received his Dr. rer. nat. (Ph.D.) in 2011 from the University of Bonn, Germany, in experimental elementary particle physics at the ATLAS experiment at CERN, Geneva. In 2012 he joined Corporate Research of Robert Bosch GmbH, where he has been involved in various data mining and machine learning activities related to driver assistance and automated driving.



**Hanna Ziesche** is a research scientist at the Bosch Center for Artificial Intelligence working on robotics and information theoretic deep reinforcement learning. She received her Dr. rer. nat. (Ph.D) in 2016 from the University of Karlsruhe, Germany, in theoretical particle physics. In 2017 she joined Robert Bosch GmbH, where she has been involved in various projects on machine learning and reinforcement learning topics.



**Waleed Ahmed** received his M.Sc degree in Automation and Robotics in 2018 from the Technical University of Dortmund, Germany, with a focus on robotics and machine learning. Since 2018, he is a development engineer at the Bosch Cognitive Systems Group with a focus on Automated Driving. He has been involved in various machine learning activities for automated driving and identification of driving strategies for driver assistance systems.



**Lutz Bürkle** received his Dr. rer. nat. (Ph.D.) in physics from the University of Freiburg, Germany, in 2001. From 1997 he was a Research Scientist at the Fraunhofer Institute of Applied Solid State Physics in Freiburg, Germany. In 2002 he joined Robert Bosch GmbH, where he has been involved in the development of various driver assistant and automated driving systems. He is currently a project manager at Bosch Corporate Research in Renningen, Germany.



**Claudius Gläser** received the Diploma degree in computer science from the Technical University of Ilmenau, Germany, in 2006, and the Dr.-Ing. (Ph.D.) degree from Bielefeld University, Germany, in 2012. From 2006 he was a Research Scientist with the Honda Research Institute Europe GmbH, Offenbach/Main, Germany, working in the fields of speech processing and language understanding for humanoid robots. In 2011, he joined the Corporate Research of Robert Bosch GmbH in Renningen, Germany, where he developed perception algorithms for driver assistance and highly automated driving functions. He is currently senior expert for sensor data fusion in autonomous systems. His research interests include environment perception, multimodal sensor data fusion, multi object tracking, and machine learning for highly automated driving.